Available online at www.sciencedirect.com

Chemical Engineering Research and Design

journal homepage: www.elsevier.com/locate/cherd

A numerical analysis of the influence of material properties on dry powder coating performance

Marv J. Khala[a,*], Colin Hare[a], Vikram Karde[b], Jerry Y.Y. Heng[b,c]

[a] School of Engineering, Newcastle University, Newcastle upon Tyne NE1 7RU, UK
[b] Department of Chemical Engineering, Imperial College London, London SW7 2AZ, UK
[c] Institute for Molecular Science and Engineering, Imperial College London, London SW7 2AZ, UK

ARTICLE INFO

Article history:
Received 28 October 2022
Received in revised form 13 March 2023
Accepted 14 March 2023
Available online 17 March 2023

Keywords:
Dry powder coating
DEM
Granular Bond number
Material properties

ABSTRACT

Dry powder coating is a preferable surface modification technique over the traditional aqueous coating technique due to reduced energy waste and less environmental impact. Despite the benefits of dry powder coating, excessive amount of coating powder energy input is often applied to ensure sufficient coating is achieved. In this study, the Discrete Element Method (DEM) is utilised to assess the influence of material properties on dry coating efficiency in a blade-driven system. Granular Bond number is used to predict coating performance based on multiple simulations with varied material properties. This provides insight on the optimal range of material properties (size ratio, density ratio and surface energy) to achieve uniformly distributed coatings, thus providing precise control of the quantity of coating material required and minimising energy consumption.

1. Introduction

Dry powder coating has been widely used as a surface modification technique to create particles with desired functionalities or manufacturability such as enhanced flowability, by reducing separation distance between host particles, and controlled release of pharmaceutical drugs. The dry coating process is favourable over the conventional solvent-based coating due to zero emission of volatile organic solvents and lower energy consumption as the subsequent drying process is not required, thus reducing processing time and costs. Moreover, dry coating is suitable for moisture sensitive Active Pharmaceutical Ingredients (APIs). Various techniques have been used for the dry deposition of guest particles onto the surface of host particles such as electrostatic coating (Jaber et al., 2021; Jing et al., 2022; Yang et al., 2015), mechanofusion (Qu et al., 2015; Zhou et al., 2010, 2011), hybridizer (Yang et al., 2005), rotating tumbler (Gärtner et al., 2021), resonance acoustic mixing (Kunnath et al., 2021), magnetic-assisted impact coating (Chen et al., 2010; Pfeffer et al., 2001; Yang et al., 2005), milling (Capece et al., 2021; Karde et al., 2015; Mullarney et al., 2011; Wei et al., 2017; Zhang et al., 2009), fluidised bed (Smikalla et al., 2011), high shear mixing (Karde et al., 2023) and pan coating (Fulchini et al., 2017). Detailed reviews of the different techniques are provided by Sharma and Setia (2019), Sauer et al. (2013) and Pfeffer et al. (2001). For the high shear processes, the dry coating process involves mechanical breakage and dispersion of agglomerates, collision with other particles and subsequent adhesion of fine (guest) particles onto the surface of carrier (host) particles. The deagglomeration of guest particles is primarily governed by the interparticle forces such as surface energy and van der Waals forces. As such, the mechanical energy imparted on the powder bed results in high shear stresses, which promote the breakage of agglomerates and dispersion of primary guest particles. Repeated high

Abbreviations: DEM, Discrete Element Method; API, Active Pharmaceutical Ingredients; SAC, Surface Area Coverage; IGC, Inverse Gas Chromatography

* Corresponding author.
E-mail address: marv.khala@newcastle.ac.uk (M.J. Khala).

https://doi.org/10.1016/j.cherd.2023.03.028

impact collisional forces promote the adhesion of the guest particles onto the surface of host particles until the desired mixture homogeneity or surface area coverage is achieved by forming a discrete, continuous or film surface layer on the host particles. Despite the proven success of dry powder coating in many industrial applications, excessive amount of coating powder and energy input are typically required to achieve desired coating uniformity, where all target particles are sufficiently coated. Therefore, fundamental understanding of the factors governing dry powder coating is required to improve the process efficiency.

Several numerical studies have been carried out to elucidate the dry powder coating mechanisms (Alonso et al., 1989; Dave et al., 2003; Deng et al., 2018; Nguyen et al., 2016, 2014; Tamadondar et al., 2018). Tamadondar et al. (2018) carried out a DEM study on dry powder coating in a Couette cell and related the coating efficiency to the Stokes number and the ratio of cohesive to adhesive strength of particle contacts. Alonso et al. (1989) proposed a population balance model correlating particle size ratio and guest concentration to the coating quality. Although these models give some insight into the interplay between some material properties and the dry coating efficiency, more robust models are required for better understanding of the relative influence of material properties on the uniformity of dry coatings. The present study aims to examine the influence of size ratio, density ratio and surface energy on dry powder coating efficiency in a bladed high shear mixer by utilizing the Discrete Element Method (DEM to give insight on the optimal combination of material properties that give uniformly distributed coatings.

2. Methodology

The dry powder coating process was simulated using the Hertz-Mindlin-JKR model in the EDEM® software (Altair Engineering Inc.). In the Hertz-Mindlin-JKR contact model (Johnson et al., 1971), the contact normal force is given by,

$$f_n = \frac{4E^*a^3}{3R^*} - \sqrt{8\pi\Gamma E^* a^3} \tag{1}$$

where Γ is the interfacial energy, a is the radius of normal contact area, E^* and R^* are the equivalent Young's modulus and particle radius given by Eqs. (2) and (3), respectively.

$$E^* = \left(\frac{1-\nu_i^2}{E_i} + \frac{1-\nu_j^2}{E_j}\right)^{-1} \tag{2}$$

$$R^* = \frac{R_i R_j}{R_i + R_j} \tag{3}$$

where υ_i, υ_j are the Poisson's ratios, E_i, E_j are the Young's moduli, and R_i, R_j are the radii of the contacting particles. The normal overlap is given by,

$$\delta = \frac{a^2}{R^*} - \sqrt{\frac{4\pi\Gamma a}{E^*}} \tag{4}$$

The dry coating system consists of a 25 mm diameter vessel and a 23.5 mm diameter impeller (with an inclination towards the tip) of the FT4 powder rheometer. A pre-segregated granular bed of host and guest particles was created by initially generating host particles with a bed height of 13 mm. A bed height of 13 mm was selected based on the swept volume by the blade such that there are no significant dead zones below and above the blade, which has a maximum vertical height of 6.14 mm. Thereafter, guest particles of 2 % w/w concentration are generated and collected on a circular plate positioned at 0.5 mm above the host particles to form a thin layer of guest particles. The circular plate is then removed to allow the thin layer of guest particles to settle on the upper free layer of host particles under gravity as illustrated in Fig. 1. The impeller is rotated in a fixed vertical position at a rotational speed of 244 rpm for a duration of 5 blade revolutions. The material and interaction properties used in the simulations are given in Table 1. The effects of material properties (size ratio, density ratio and surface energy) on the surface area coverage (SAC) are evaluated. A minimum particle size ratio of 10 is investigated since particle size ratios less than 10 are unlikely for a dry coating process.

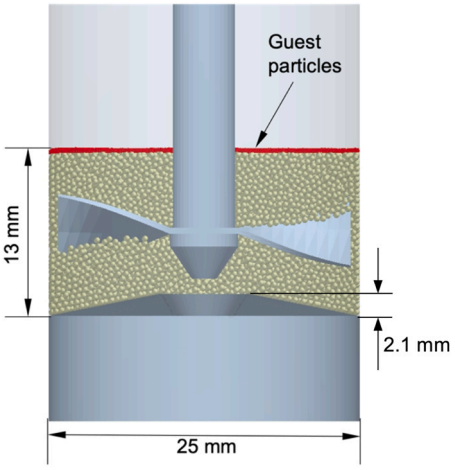

Fig. 1 – Geometries and bed configuration used in the simulations.

The SAC is defined as the ratio of the total projected area of guest particles to the maximum available host surface area, expressed as,

$$\mathrm{SAC} = \frac{1}{N_h}\sum_{n=1}^{N_h}\frac{n_g A_{p,g}}{\xi S_h} \times 100 \tag{5}$$

where N_h is the total number of host particles, n_g is the number of guest particles per host particle, $A_{p,g}$ is the projected area of the guest particles, S_h is the surface area of the host particle, the factor $\xi = 0.906$ (Thue, 1910) represents the highest density hexagonal packing arrangement of the spherical guest particles i.e., the maximum available surface area for coating. The maximum achievable SAC in an ideal system with uniformly distributed coatings i.e., ratio of total projected area of guest particles to total available surface area of host particles, given by

$$\mathrm{SAC}_{\max} = \frac{\sum_{i=1}^{N_g} r_{g,i}^2}{\sum_{j=1}^{N_h} 4\xi r_{h,j}^2} \tag{6}$$

To allow comparison to ideal coating, surface area coverage (Eq. 5) is normalised by the maximum achievable SAC (Eq. 6). The granular Bond number, Bo, is defined as the ratio of cohesive forces to the gravitational forces, expressed as,

$$Bo = \frac{f_c}{f_w} \tag{7}$$

where f_c is the cohesive force between two particles according to the JKR contact theory (Johnson et al., 1971), given by Eq. (8) and f_w is the harmonic mean of the gravitational forces given by Eq. (9).

Table 1 – Material and interaction properties used in the simulations.

Property	Value
Mean guest diameter (mm)	0.05–0.2 ± 5 %
Mean host diameter (mm)	0.5–2 ± 5 %
Particle density (kg/m^3)	2500–10000
Geometry density (kg/m^3)	7800
Particle Poisson's ratio (-)	0.25
Geometry Poisson's ratio (-)	0.3
Young's modulus (GPa)	0.05
Particle-particle sliding friction coefficient (-)	0.3
Particle-geometry sliding friction coefficient (-)	0.2
Particle-particle rolling friction coefficient (-)	0.01
Particle-geometry rolling friction coefficient (-)	0.01
Particle-particle restitution coefficient (-)	0.8
Particle-geometry restitution coefficient (-)	0.9
Particle-particle surface energy, Γ (mJ/m^2)	43–129
Particle-geometry surface energy, Γ (mJ/m^2)	0

$$f_c = \frac{3\pi R^* \Gamma}{2} \tag{8}$$

$$f_w = \frac{2w_g w_h}{w_g + w_h} \tag{9}$$

where w_g and w_h are the weights of the contacting guest and host particles.

3. Results and discussion

3.1. *Influence of size ratio*

Fig. 2 shows the influence of the absolute particle size on the evolution of SAC_{norm} for systems with $r_h/r_g = 10$, $\rho_h = \rho_g = 2500$ kg/m^3 and $\Gamma = 43$ mJ/m^2. For $r_g \leq 0.05$ mm, SAC_{norm} increases with number of blade revolutions and approaches a steady state. For $r_g = 0.06$ mm and 0.065 mm, SAC_{norm} initially increases before reducing, suggesting that some guest particles that initially coat the hosts are dislodged upon further agitation. For $r_g > 0.065$ mm, SAC_{norm} decreases with number of blade revolutions indicating poor coating. The initial SAC_{norm} is non-zero for $r_g > 0.065$ mm, which can be attributed to percolation of guest particles during the vessel filling process before the blade rotation is initiated. This percolation phenomenon was much less significant for $r_g \leq 0.065$ mm, with decreasing significance for smaller host/guest particles. This can be observed by lower values of initial SAC_{norm} for smaller host/guest particles. Since the size ratio and interface energy are the same in all cases, the prevalence of this percolation problem, and subsequently the coating performance, is dictated by the granular Bond number shown in Fig. 3. For the purposes of defining a threshold for coating performance, we define cases where SAC_{norm} initially increases to be good coating, and cases where it decreases to be poor coating. On this basis, from Fig. 2 the coating performance is classified to transition from good to poor for 0.065 mm < r_g < 0.075 mm, which corresponds to Bo = 160–212. This range of Bo is considered to be the critical threshold, above and below which good and poor coating occur, respectively. It can be observed in Fig. 3 that Bo is predominantly influenced by guest particle size, with host

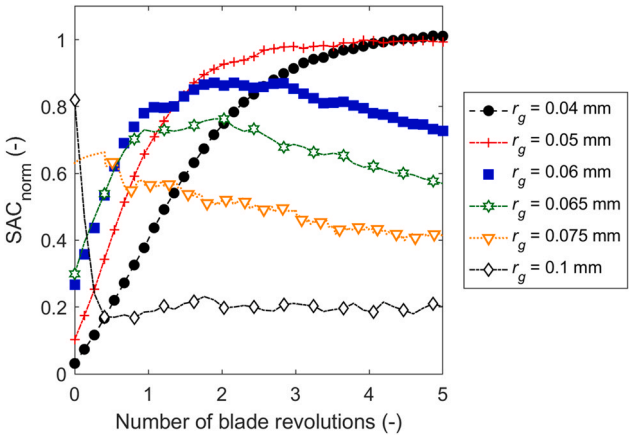

Fig. 2 – Evolution of SAC with mixing time for $r_h/r_g = 10$ with different absolute particle size of guest and host particles where $\Gamma = 43$ mJ/m^2 and $\rho_h = \rho_g = 2500$ kg/m^3.

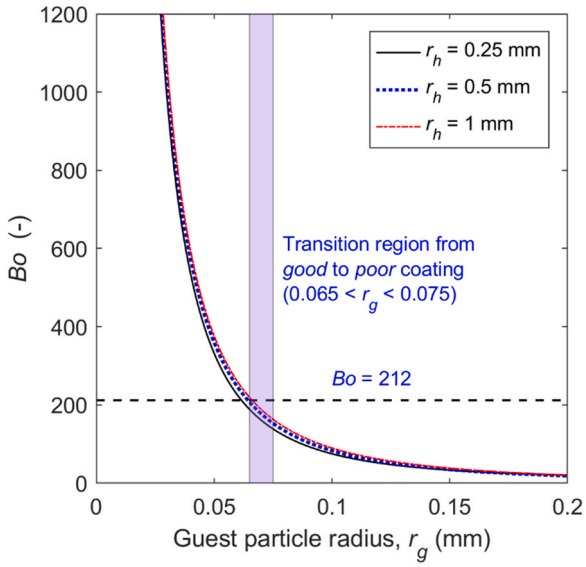

Fig. 3 – Effect of guest particle size on granular Bond number between host and guest particles according to Eq. 7 where $\Gamma = 43$ mJ/m^2 and $\rho_h = \rho_g = 2500$ kg/m^3.

size having negligible effect. This can be explained by Eqs. 3, 7–9, whereby f_w, R^* and subsequently f_c are more strongly influenced by guest particle size.

Fig. 4 shows the influence of particle size ratio on the evolution of SAC_{norm} for fixed host particle sizes of 0.5 and 1.0 mm where $\Gamma = 43$ mJ/m^2 and $\rho_h = \rho_g = 2500$ kg/m^3. For size ratios $r_h/r_g = 10$ and 20, where $r_h = 0.5$ mm, SAC_{norm} increases with number of blade revolutions, signifying good coating. However, there is a subsequent decrease of SAC_{norm} after 5 blade revolutions for $r_h/r_g = 10$, suggesting excessive energy input leads to detachment of guest particles from host surface. The rate of increase in SAC_{norm} is greater for $r_h/r_g = 10$ than $r_h/r_g = 20$, this is despite the greater Bond number for the latter (Bo = 359 and 1503, respectively). This is due to the smaller guest particles for $r_h/r_g = 20$ being more cohesive, thus requiring a greater force to separate them from each other and disperse them.

For size ratios $r_h/r_g = 10$ and 15, where $r_h = 1.0$ mm, SAC_{norm} decreases with number of blade revolutions indicating poor coating performance, whereas, for $r_h/r_g = 17.5$ and 20, SAC_{norm} initially increases with number of blade revolutions, which indicates good coating performance. The

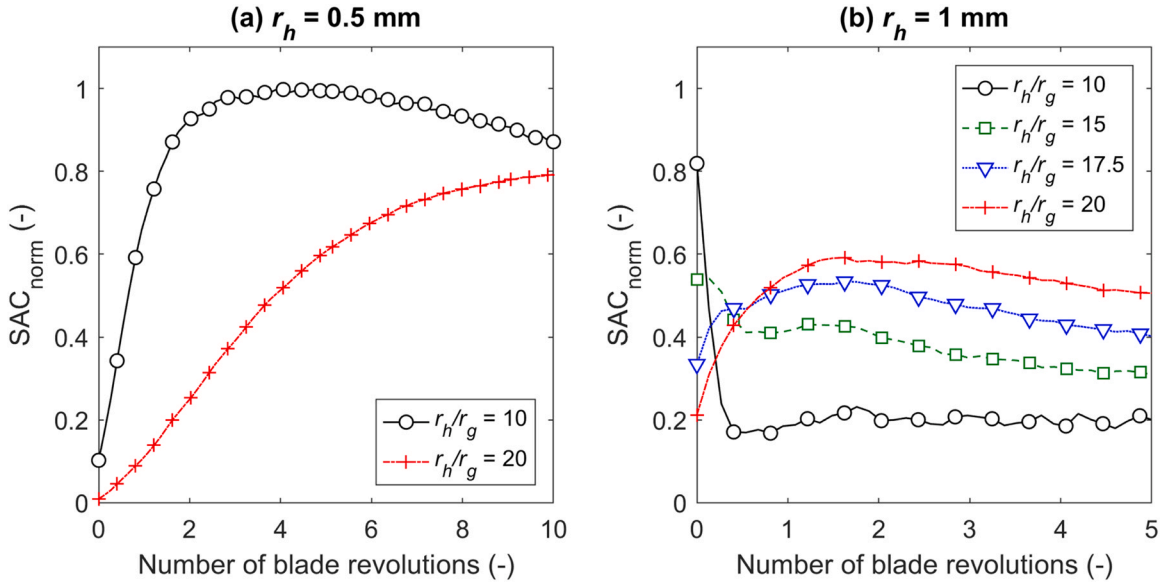

Fig. 4 – Effect of particle size ratio on SAC$_{norm}$ for (a) r_h = 0.5 mm and (b) r_h = 1.0 mm where Γ = 43 mJ/m^2 and $\rho_h = \rho_g$ = 2500 kg/m^3.

subsequent decrease in SAC$_{norm}$ for r_h/r_g = 17.5 and 20 suggests that segregation occurs due to guest detachment from host surfaces, caused by the excess energy input. For r_h/r_g = 17.5 and 20, Bo = 285 and 376, respectively, which exceed the minimum threshold for good coating performance ($160 < Bo < 212$). However, for r_h/r_g = 10 and 15, poor coating performance is observed since Bo = 90 and 208, respectively, which fall below or within the threshold limit.

Fig. 5 shows the probability density of SAC$_{norm}$ for different size ratios after 5 blade revolutions. A slightly greater variance of SAC is observed for r_h/r_g = 10 (where r_h = 0.5 mm) than for r_h/r_g = 20, which suggests more uniformly distributed coatings at r_h/r_g = 20 albeit with similar proportion of uncoated host particles for both size ratios. For r_h = 1.0 mm, a greater proportion of host particles are coated at r_h/r_g = 20 than at r_h/r_g = 10 due to better mixing and adherence of guest particles to host surfaces as shown by the distribution of guest particles depicted in Fig. 6. For r_h/r_g = 10, most of the guest particles settle and accumulate at the bottom of the vessel due to poor adhesion to host particles.

3.2. *Influence of density ratio*

Fig. 7 shows the effect of density ratio, expressed as ratio of guest particle density to host particle density, on the evolution of SAC$_{norm}$ for ρ_h = 2500 kg/m^3, r_h = 0.5 mm, r_g = 0.05 mm and Γ = 43 mJ/m^2. For $\rho_g/\rho_h < 1$, SAC$_{norm}$ increases with increasing density ratio whereas for $\rho_g/\rho_h > 1$, SAC$_{norm}$ decreases with increasing density ratio. The ratio of cohesive forces to gravitational forces is much higher for the cases with $\rho_g/\rho_h < 1$ as indicated by the granular Bond number in Fig. 8, as such the dominant interparticle forces reduce the dispersion rate and consequently, the coating rate. For ρ_g/ρ_h = 1, SAC$_{norm}$ increases with number of blade revolutions up

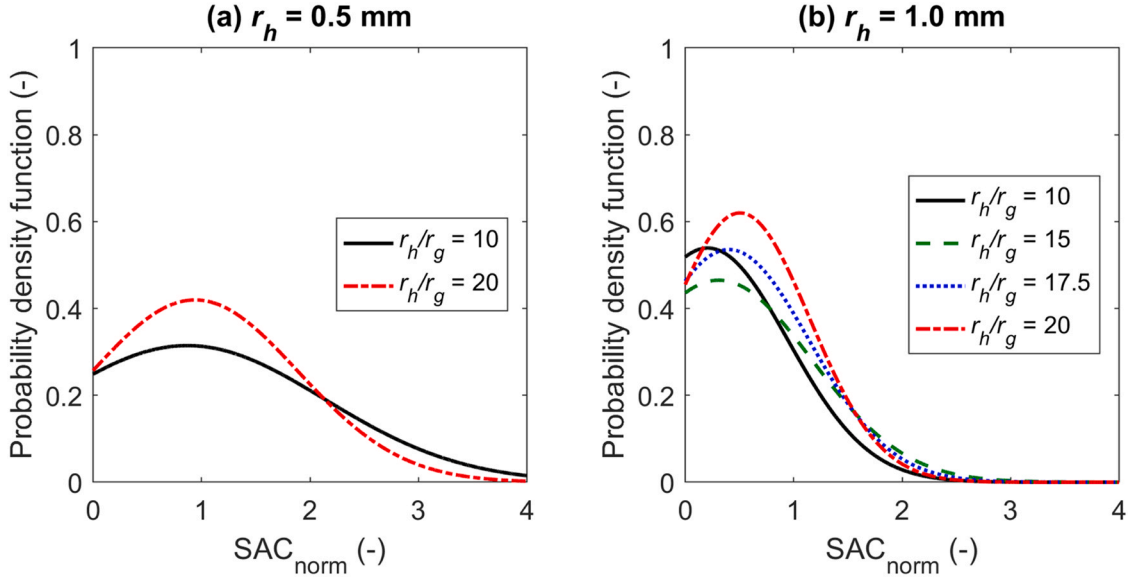

Fig. 5 – Distribution of SAC$_{norm}$ for different size ratios where (a) r_h = 0.5 mm and (b) r_h = 1.0 mm for Γ = 43 mJ/m^2 and $\rho_h = \rho_g$ = 2500 kg/m^3.

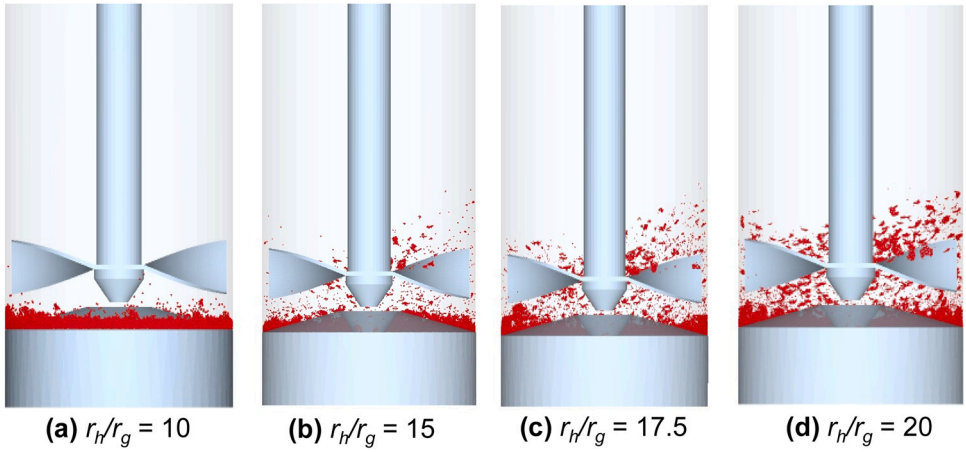

Fig. 6 – Distribution of guest particles for different size ratios after 5 blade revolutions for r_h = 1.0 mm, Γ = 43 mJ/m^2 and $\rho_h = \rho_g$ = 2500 kg/m^3.

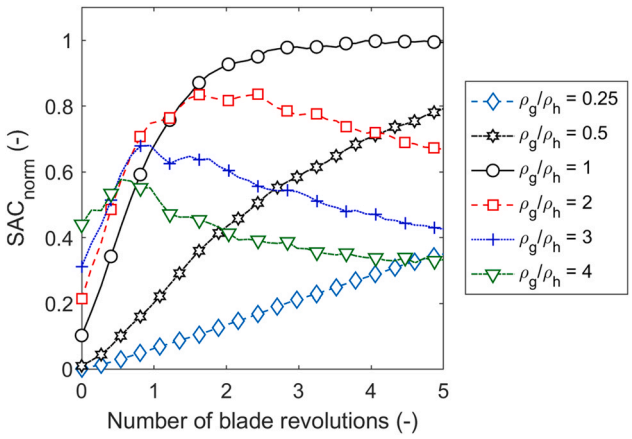

Fig. 7 – Effect of density ratio on SAC$_{norm}$ for ρ_h = 2500 kg/m^3, r_h = 0.5 mm, r_g = 0.05 mm and Γ = 43 mJ/m^2.

to a maximum of unity before plateauing, indicating good coating performance. The plateauing of SAC$_{norm}$ indicates good coating stability. The coating performance becomes progressively poorer with an increase of density ratio beyond unity. Fig. 8 shows that the granular Bond number for ρ_g/ρ_h = 2 is 180, which falls within the threshold limit of 160 < *Bo* < 212, and thus explains the short duration of the steady-state period (coating stability) before the subsequent decrease in SAC. The granular Bond number for ρ_g/ρ_h = 3 and 4 is below the threshold limit and the transient peak SAC reached is not maintained. The short-lived transient peak SAC is caused by the initial bed dilation as the blades begin to rotate leading to instantaneous guest dispersal and percolation through the bed. Since the ratio of cohesive forces to gravitational forces is much lower in these cases, guest particles are very weakly adhered to host surfaces and therefore are easily and rapidly detached from the host surfaces upon further bed agitation.

For very dense guest particles, axial dispersion is faster due to increased gravitational forces, therefore, the percolation rate is higher as indicated by the greater magnitude of axial particle velocities for higher particle densities in Fig. 9. The distribution of SAC$_{norm}$ for different density ratios is shown in Fig. 10. Lower density ratios exhibit more homogeneous distribution of SAC$_{norm}$ than higher density ratios due to better mixing. This is clearly demonstrated in Fig. 11,

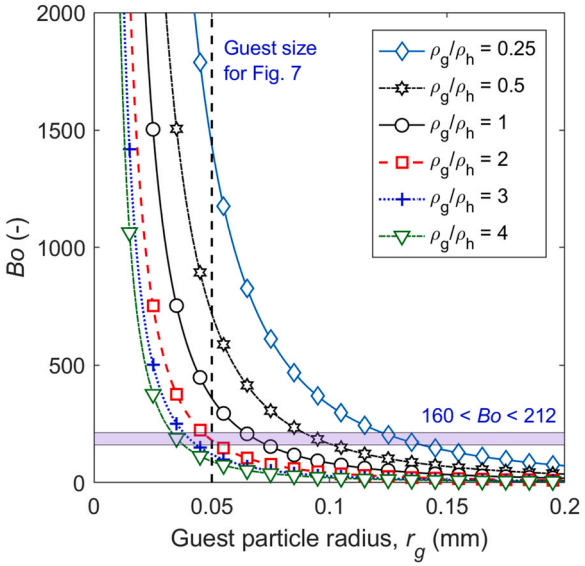

Fig. 8 – Effect of density ratio on granular Bond number according to Eq. 7 for ρ_h = 2500 kg/m^3, r_h = 0.5 mm and Γ mJ/m^2.

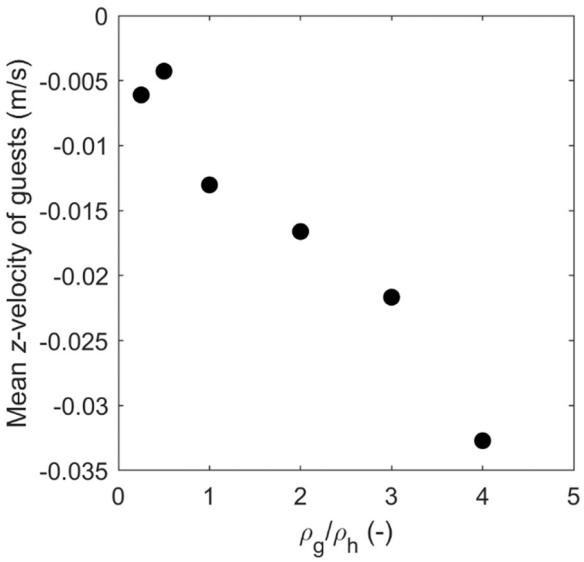

Fig. 9 – Variation of mean axial velocity of guest particles with density ratio for ρ_h = 2500 kg/m^3, r_h = 0.5 mm, r_g = 0.05 mm and Γ = 43 mJ/m^2.

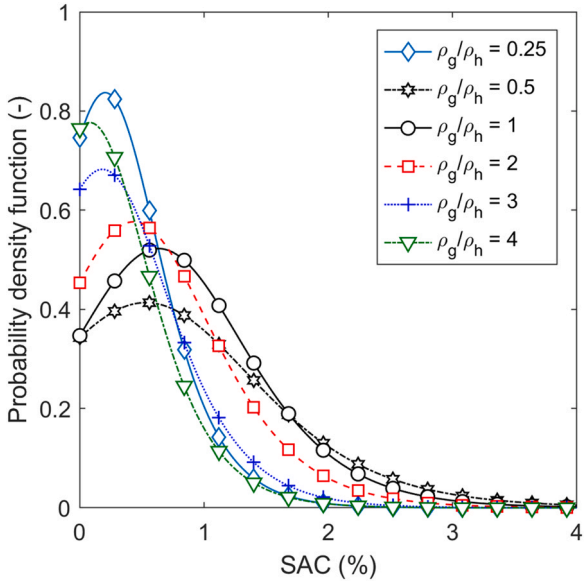

Fig. 10 – Distribution of SAC for different density ratios for ρ_h = 2500 kg/m^3, r_h = 0.5 mm, r_g = 0.05 mm and Γ = 43 mJ/m^2.

which shows that a greater proportion of guest particles segregate to the bottom of the vessel at higher density ratios after 5 blade revolutions.

3.3. *Influence of surface energy*

Fig. 12 shows the effect of surface energy on SAC_{norm} for different density ratios where ρ_h = 2500 kg/m^3, r_h = 0.5 mm, r_g = 0.05 mm. For ρ_g/ρ_h = 1, the rate of increment of SAC_{norm} decreases with increasing surface energy. This behaviour can be partially attributed to the increase in the cohesive inter-particle contact forces (see Fig. 13(a)) thus requiring higher shear stress or prolonged mixing time to break up and disperse the guest agglomerates. Furthermore, the increased SAC_{norm} for lower surface energies is due to guest particle agglomerates being more easily dispersed leading to more free guest particles being available to coat the hosts. This is indicated in Fig. 13(b), which shows that for lower surface energies the number of guest-guest contacts are reduced.

Fig. 12 also shows that for ρ_g/ρ_h = 2, doubling the surface energy from 43 to 86 mJ/m^2 improves the coating as the segregation phenomenon is mitigated due to stronger affinity of guest particles to host surfaces. This remains the case even for excess energy input, as SAC_{norm} approaches unity after 3 blade revolutions and does not decrease with further revolutions. However, a further increase in the surface energy to 129 mJ/m^2 leads to a decrease in SAC_{norm} due to the guests being more difficult to disperse. Similarly, for ρ_g/ρ_h = 3 and 4, a surface energy of 43 mJ/m^2 leads to poor coating performance, whereas surface energies of 86 and 129 mJ/m^2 provide good coating performance. This suggests that for a given granular system, there exists a threshold range of surface energies, in which optimum coating performance is achieved; if the surface energy is too low the guests exist as discrete free particles and easily bypass the hosts or easily detach from host surfaces and percolate through the bed, whereas if surface energy is too high deagglomeration and dispersal of guests requires much more energy input and the coating process is slow.

3.4. *Influence of size distribution*

Guest and host particles with various size distributions were simulated for $\rho_h = \rho_g$ = 2500 kg/m^3 and Γ = 43 mJ/m^2. In these cases, a Gaussian distribution with the same mean particle sizes (r_h = 0.5 mm, r_g = 0.05 mm) but varying values of standard deviation as a fraction of the mean, σ, are used, as shown in Fig. 14. Fig. 15 shows the effect of host and guest size distribution on SAC_{norm}. For a normal Gaussian distribution of host particle size with σ_h = 0.1, there is an apparent decrease in SAC_{norm} in comparison to the case with σ_h = 0.05 and σ_g= 0.05. This can be attributed to a 1.5 % increase in available host surface area for coating. For a wider distribution of host particle size (σ_h = 0.3), there is an even greater reduction in SAC_{norm} by approximately 14 % in comparison to the case with σ_h = 0.05 and σ_g = 0.05, which correspond to a 6.9 % increase in available host surface area. For the case with σ_h = 0 and σ_g = 0.1, the total guest projected area increases by 0.7 % relative to the case with σ_h = 0 and σ_g = 0.05, hence an increase in SAC_{norm}. However, similar evolution of SAC_{norm} is observed for the cases where both guest and host particles have polydispersity and the cases where only the host particles have

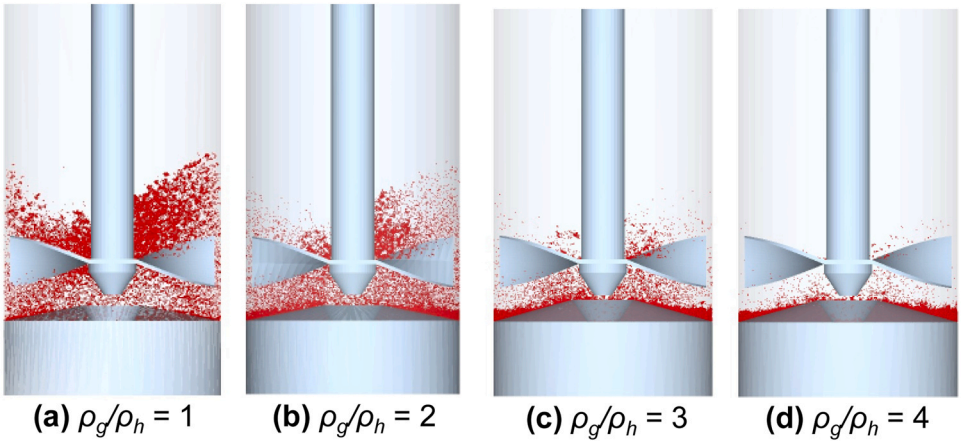

Fig. 11 – Distribution of guest particles for different density ratios for ρ_h = 2500 kg/m^3, r_h = 0.5 mm, r_g = 0.05 mm and Γ = 43 mJ/m^2.

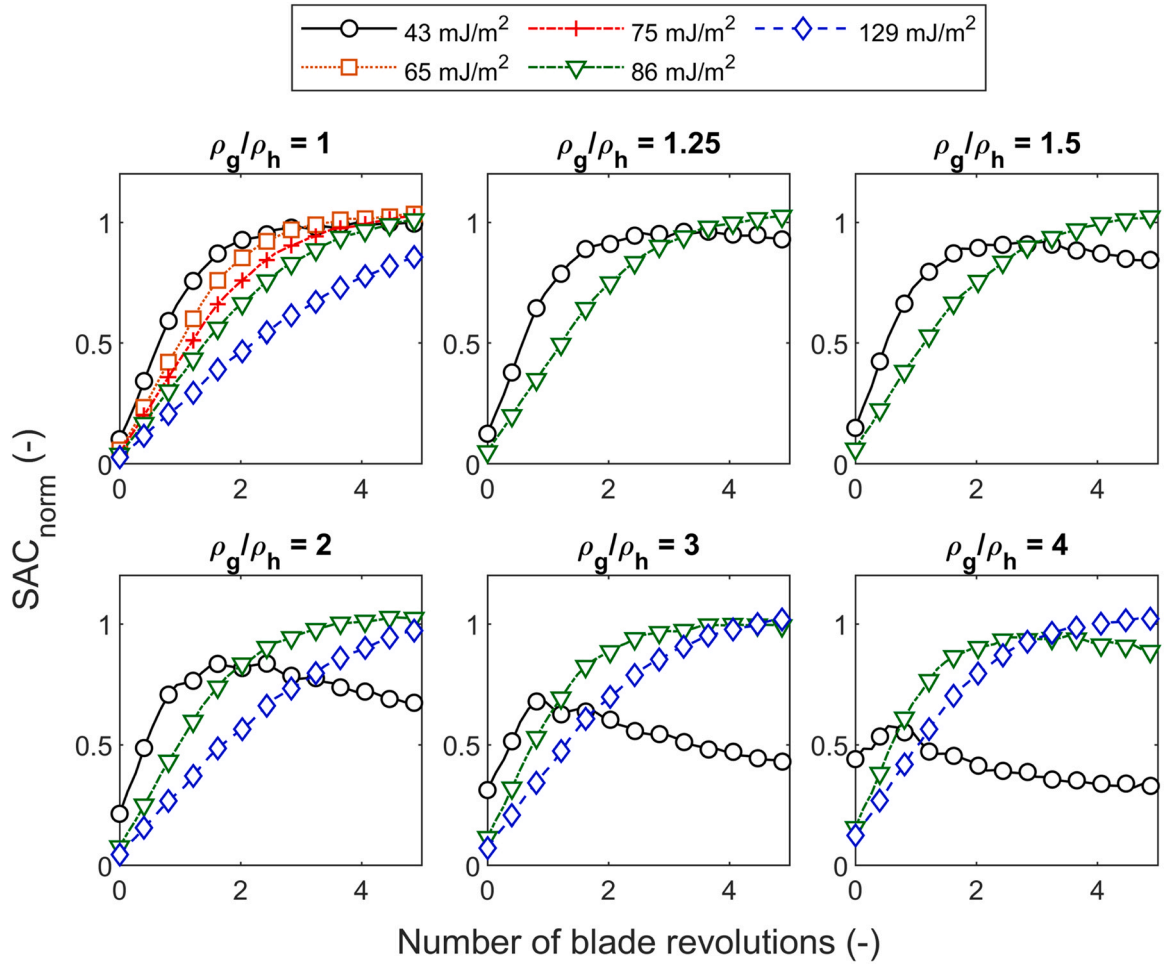

Fig. 12 – Effect of interfacial energy on SAC for $\rho_h = 2500\ kg/m^3$, $r_h = 0.5\ mm$ and $r_g = 0.05\ mm$.

polydispersity. This is due to a relatively greater increase in total host surface area in contrast to the total guest projected area for the same variance. It can therefore be concluded that guest particle size distribution has limited effect on coating performance, whereas increased polydispersity of the hosts worsens the coating performance.

3.5. *Coating performance based on granular Bond number*

Fig. 16 shows granular Bond number as a function of size and density ratios, where only the guest particle size (monodisperse) and density are varied for $\rho_h = 2500\ kg/m^3$ and Γ

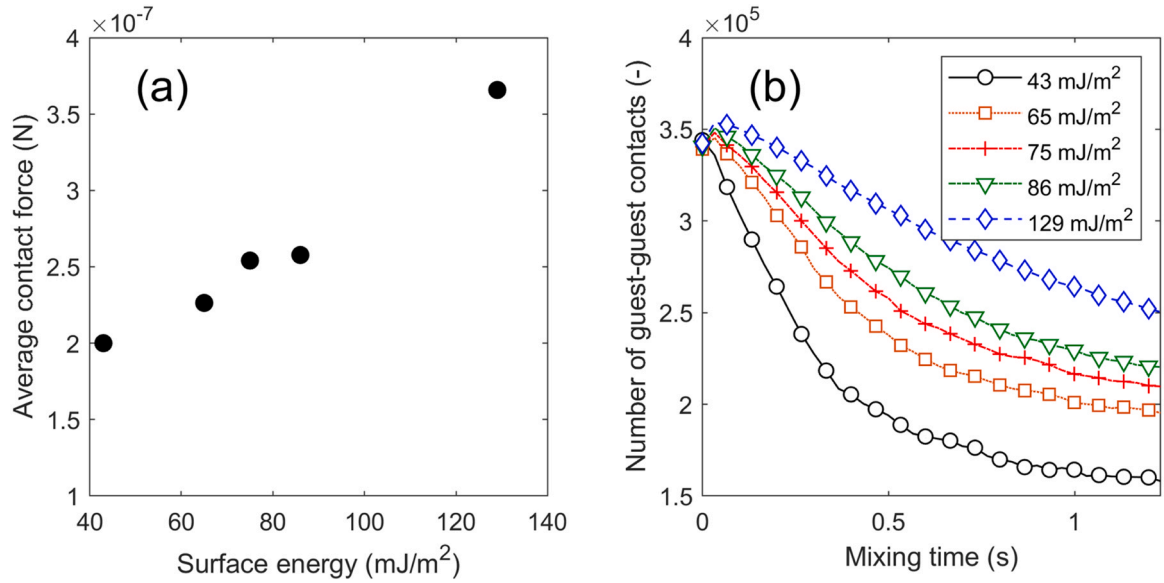

Fig. 13 – (a) Average guest-host contact forces as a function of surface energy and (b) evolution of guest-guest contacts for a range of surface energies for $r_h = 0.5\ mm$, $r_g = 0.05\ mm$ and $\rho_h = \rho_g = 2500\ kg/m^3$.

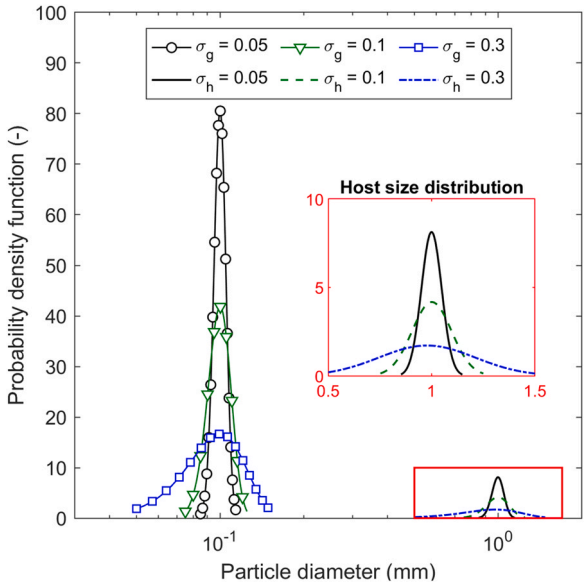

Fig. 14 – Particle size distribution of the simulated guest and host particles.

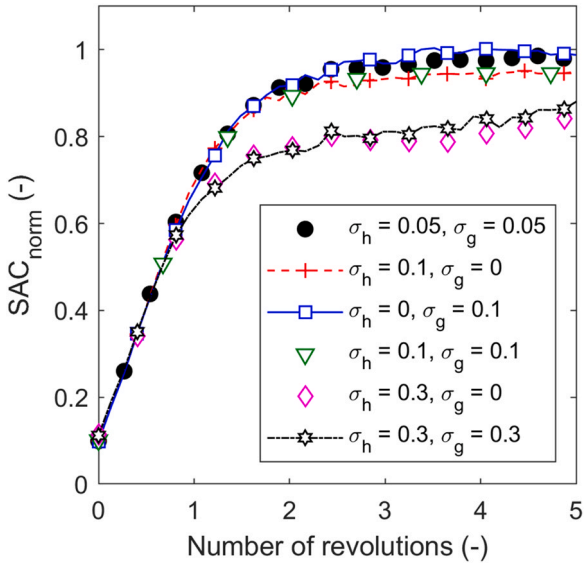

Fig. 15 – Effect of size distribution on SAC_{norm} for r_h = 0.5 mm, r_g = 0.05 mm, $\rho_h = \rho_g$ = 2500 kg/m³ and Γ = 43 mJ/m².

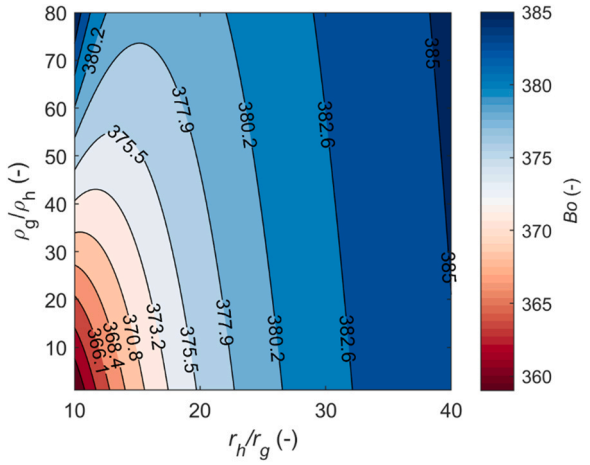

Fig. 17 – Granular Bond number as a function of particle size ratio and density ratio for r_g = 0.05 mm, ρ_g = 2500 kg/m³ and Γ = 43 mJ/m².

= 43 mJ/m². Granular Bond numbers beyond the transition range of 160 < *Bo* < 212 represent good coating performance as previously discussed in Sections 3.1–3.3. The coloured circular markers represent the simulation results, where the shades represent the maximum SAC_{norm} achieved after 5 blade revolutions. The threshold range for *Bo*, represented by the black solid lines, appears to adequately define the regions of good and poor coating, as confirmed by the simulation results, where SAC_{norm} is typically < 0.65 for the *Bo* values below the threshold and > 0.7 above the threshold for the finer particle system (r_h = 0.5 mm). For the coarser particle system (r_h = 1 mm), SAC_{norm} is typically < 0.3 for the *Bo* values below the threshold and > 0.35 above the threshold. This difference can be attributed to the number of particles in each system; the finer particle system has a greater number of guest and host particles and thus denser than the coarser particle system. Upon agitation, a greater number of particles in the coarser particle system become airborne resulting in greater bed dilation and percolation rate of guest particles, which reduces the likelihood of guest particles coating the host surfaces.

Fig. 17 shows granular Bond number as a function of size and density ratios, where only the host particle density and size are varied for r_g = 0.05 mm, ρ_g = 2500 kg/m³ and

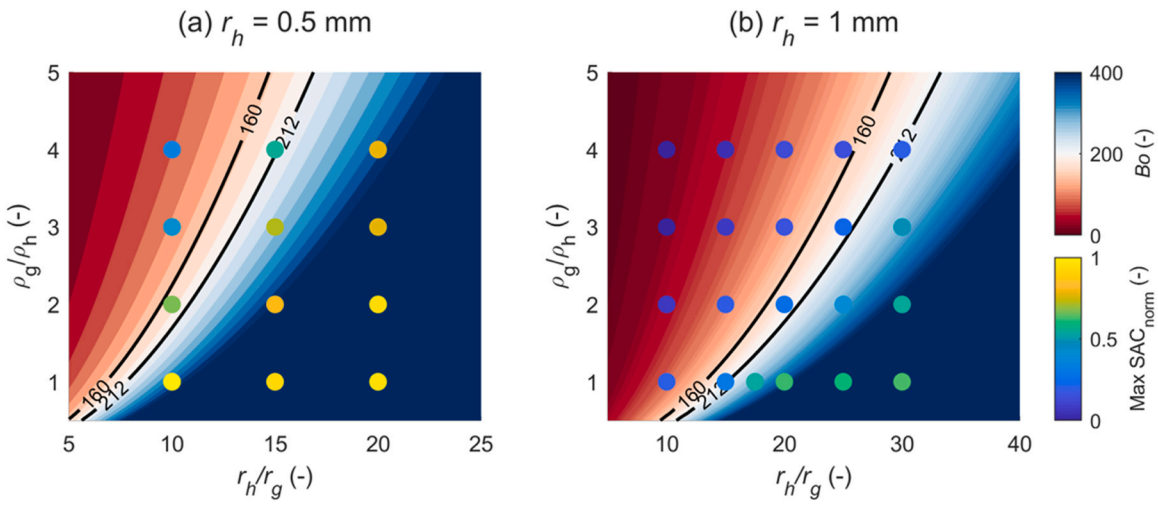

Fig. 16 – Granular Bond number as a function of particle size ratio and density ratio for (a) r_h = 0.5 mm and (b) r_h = 1 mm at ρ_h = 2500 kg/m³ and Γ = 43 mJ/m².

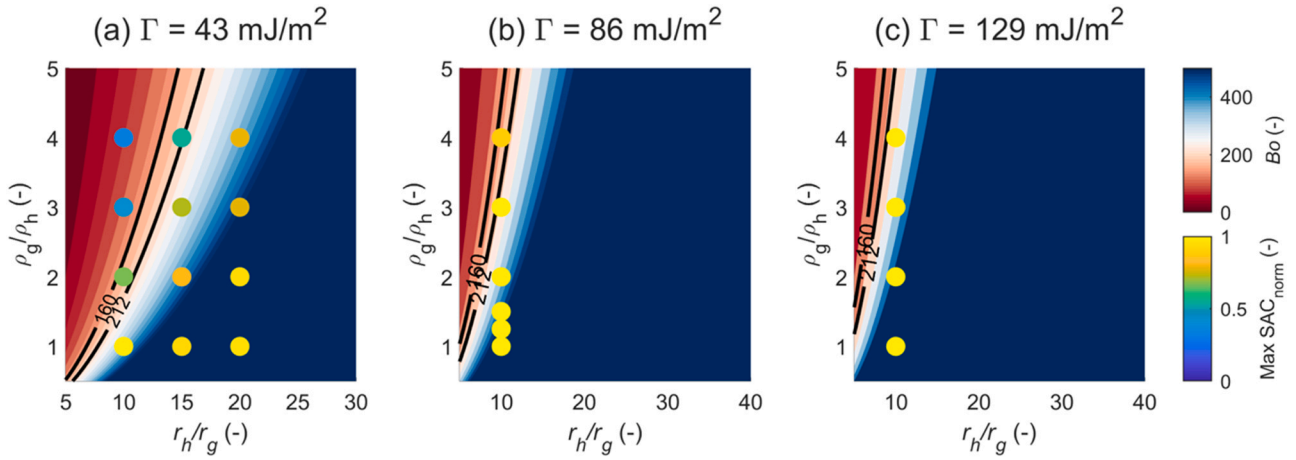

Fig. 18 – Granular Bond number as a function of particle size ratio and density ratio for (a) 43 mJ/m^2, (b) 86 mJ/m^2 and (c) 129 mJ/m^2 at r_h = 0.5 mm and ρ_h = 2500 kg/m^3.

Γ = 43 mJ/m^2. Significantly higher host density ratios ($\rho_g/\rho_h > 40$) and size ratios ($r_h/r_g > 20$) are required for a notable change in the granular Bond number. This suggests that the guest particle size and density have a much greater effect on the granular Bond number in comparison to the host particle size and density. Fig. 18 shows granular Bond number as a function of size and density ratios for different surface energies and SAC_{norm} for several simulations with r_h = 0.5 mm and ρ_h = 2500 kg/m^3. For Γ = 43 mJ/m^2, the threshold range for *Bo* appears to adequately define the regions of good and poor coating, with $SAC_{norm} > 0.7$ above the threshold and < 0.7 below the threshold. Increasing the surface energy improves coating performance for a given size and density ratio, however, for very high surface energies, the rate of increment of SAC_{norm} is reduced, as shown in Fig. 12.

It should be noted that the values of SAC_{norm} shown in Fig. 18 correspond only to the coating after 5 impeller revolutions, however in order to optimise dry coating processes it is important to consider the influence impeller speed and mixing time have on coating performance. This aspect will be addressed in further research. The validity of the model results shown in Figs. 16 and 18 can be scrutinized using literature data available on dry particle coating of pharmaceutical powders (Capece et al., 2014; Kunnath et al., 2021). The surface energy for host and guest materials was measured using Inverse Gas Chromatography (IGC). It is important to note that in the studies by (Capece et al., 2014) and (Kunnath et al., 2021), the cohesive force used for calculating the granular Bond number is based on the van der Waals force of attraction between host particles whereas in our work the cohesive force is calculated according to the JKR contact theory between host and guest particles (see Eqs. 7 and 8). For all cases investigated involving combinations of a range of pharmaceutical powders with silica, alumina and titania, good coating performance was achieved since $Bo >> 212$ ($10^3 < Bo < 10^{11}$).

4. Conclusions

Dry coating performance in a bladed mixer has been evaluated as a function of material properties. For a fixed size ratio, increasing the size of guest and host particles reduces the SAC due to poor sticking induced by the increase in gravitational forces relative to cohesive forces for the guest particles. Increasing the span of distribution of host particles reduces SAC_{norm} due to an increase in the available total host surface area. Conversely, increasing the span of distribution of guest particles leads to an increase in SAC_{norm} due to an increase in total projected area of guest particles. An increase in guest particle density reduces SAC_{norm} due to the faster percolation of guests through the bed, and the greater adhesive force required for them to stick to host particles. SAC_{norm} increases with surface energy when it is increased from a low value; however, very high surface energies negate the dispersibility of the agglomerated guest particles resulting in greater energy input being required to overcome the otherwise poor coating performance.

Granular Bond number, which dictates the affinity of guest particles to the surface of host particles, appears to provide an accurate characterisation of coating performance. Granular Bond number as a function of density and size ratios indicates that a threshold limit ($160 < Bo < 212$) exists, above and below which good and poor coating occur, respectively. The guest particle size has a greater influence on the granular Bond number than the host particle size, hence a greater control of coating efficiency. It should be noted that this limit may depend on the operational parameters of the system.

Declaration of Competing Interest

The authors declare that they have no known competing financial interests or personal relationships that could have appeared to influence the work reported in this paper.

Acknowledgments

The authors would like to thank the EPSRC for financial support through the grant EP/V003070/1 and EP/V003070/2. The authors would also like to thank Jamie Clayton (Freeman Technology), Vicenzino Vivacqua (Johnson Matthey), Joel Caragay (Procter & Gamble), Gerald Hebbink and Pauline Janssen (DFE Pharma) for providing their expertise in discussing this work.

References

Alonso, M., Satoh, M., Miyanami, K., 1989. Kinetics of fines transfer among carriers in powder coating. Powder Technol. 59, 217–224. https://doi.org/10.1016/0032-5910(89)80068-3

Capece, M., Borchardt, C., Jayaraman, A., 2021. Improving the effectiveness of the Comil as a dry-coating process: enabling direct compaction for high drug loading formulations. Powder Technol. 379, 617–629. https://doi.org/10.1016/J.POWTEC.2020.10.070

Capece, M., Huang, Z., To, D., Aloia, M., Muchira, C., Davé, R.N., Yu, A.B., 2014. Prediction of porosity from particle scale interactions: surface modification of fine cohesive powders. Powder Technol. 254, 103–113. https://doi.org/10.1016/J.POWTEC.2014.01.006

Chen, Y., Jallo, L., Quintanilla, M.A.S., Dave, R., 2010. Characterization of particle and bulk level cohesion reduction of surface modified fine aluminum powders. Colloids Surf. A Physicochem Eng. Asp. 361, 66–80. https://doi.org/10.1016/J.COLSURFA.2010.03.015

Dave, R., Chen, W., Mujumdar, A., Wang, W., Pfeffer, R., 2003. Numerical simulation of dry particle coating processes by the discrete element method. Adv. Powder Technol. 14, 449–470. https://doi.org/10.1163/156855203769710672

Deng, X., Zheng, K., Davé, R.N., 2018. Discrete element method based analysis of mixing and collision dynamics in adhesive mixing process. Chem. Eng. Sci. 190. https://doi.org/10.1016/j.ces.2018.06.043

Fulchini, F., Zafar, U., Hare, C., Ghadiri, M., Tantawy, H., Ahmadian, H., Poletto, M., 2017. Relationship between surface area coverage of flow-aids and flowability of cohesive particles. Powder Technol. 322, 417–427. https://doi.org/10.1016/J.POWTEC.2017.09.013

Gärtner, E., Jung, H.Y., Peter, N.J., Dehm, G., Jägle, E.A., Uhlenwinkel, V., Mädler, L., 2021. Reducing cohesion of metal powders for additive manufacturing by nanoparticle dry-coating. Powder Technol. 379, 585–595. https://doi.org/10.1016/J.POWTEC.2020.10.065

Jaber, A.A., Obaid, A.A., Advani, S.G., Gillespie, J.W., 2021. Experimental investigation of dry powder coating processing parameters on the polystyrene particle's distribution on the surface of carbon fibers. Powder Technol. 393, 461–470. https://doi.org/10.1016/J.POWTEC.2021.07.089

Jing, Z., Ma, Y., Zhu, J., 2022. Application of a novel electrostatic dry powder coating technology on capsules for enteric release. J. Drug Deliv. Sci. Technol. 68, 103058. https://doi.org/10.1016/J.JDDST.2021.103058

Johnson, K.L., Kendall, K., Roberts, A.D., 1971. Surface energy and the contact of elastic solids. Proc. R. Soc. A: Math. Phys. Eng. Sci. 324, 301–313. https://doi.org/10.1098/rspa.1971.0141

Karde, V., Khala, M.J., Hare, C., Heng, J.Y.Y., 2023. Use of shear sensitive coloured guest component to track powder mixing in adhesive binary mixtures. Powder Technol 414, 118068. https://doi.org/10.1016/j.powtec.2022.118068

Karde, V., Panda, S., Ghoroi, C., 2015. Surface modification to improve powder bulk behavior under humid conditions. Powder Technol. 278, 181–188. https://doi.org/10.1016/J.POWTEC.2015.03.025

Kunnath, K., Chen, L., Zheng, K., Davé, R.N., 2021. Assessing predictability of packing porosity and bulk density enhancements after dry coating of pharmaceutical powders. Powder Technol. 377, 709–722. https://doi.org/10.1016/J.POWTEC.2020.09.037

Mullarney, M.P., Beach, L.E., Davé, R.N., Langdon, B.A., Polizzi, M., Blackwood, D.O., 2011. Applying dry powder coatings to pharmaceutical powders using a comil for improving powder flow and bulk density. Powder Technol. 212, 397–402. https://doi.org/10.1016/J.POWTEC.2011.06.008

Nguyen, D., Rasmuson, A., Thalberg, K., Björn, I.N., 2016. The exchange of fines between carriers in adhesive particle mixing: a study using DEM simulation. Powder Technol. 288. https://doi.org/10.1016/j.powtec.2015.10.048

Nguyen, D., Rasmuson, A., Thalberg, K., Niklasson Bjorrn, I., 2014. Numerical modelling of breakage and adhesion of loose fine-particle agglomerates. Chem. Eng. Sci. 116, 91–98. https://doi.org/10.1016/J.CES.2014.04.034

Pfeffer, R., Dave, R.N., Wei, D., Ramlakhan, M., 2001. Synthesis of engineered particulates with tailored properties using dry particle coating. Powder Technol. 117, 40–67. https://doi.org/10.1016/S0032-5910(01)00314-X

Qu, L., Zhou, Q., Denman, J.A., Stewart, P.J., Hapgood, K.P., Morton, D.A.V., 2015. Influence of coating material on the flowability and dissolution of dry-coated fine ibuprofen powders. Eur. J. Pharm. Sci. 78, 264–272. https://doi.org/10.1016/J.EJPS.2015.07.016

Sauer, D., Cerea, M., Dinunzio, J., McGinity, J., 2013. Dry powder coating of pharmaceuticals: a review. Int J. Pharm. 457, 488–502. https://doi.org/10.1016/J.IJPHARM.2013.02.032

Sharma, R., Setia, G., 2019. Mechanical dry particle coating on cohesive pharmaceutical powders for improving flowability - a review. Powder Technol. 356, 458–479. https://doi.org/10.1016/J.POWTEC.2019.08.009

Smikalla, M., Mescher, A., Walzel, P., Urbanetz, N.A., 2011. Impact of excipients on coating efficiency in dry powder coating. Int J. Pharm. 405, 122–131. https://doi.org/10.1016/J.IJPHARM.2010.12.001

Tamadondar, M.R., de Martín, L., Thalberg, K., Björn, I.N., Rasmuson, A., 2018. The influence of particle interfacial energies and mixing energy on the mixture quality of the dry-coating process. Powder Technol. 338. https://doi.org/10.1016/j.powtec.2018.07.022

Thue, A., 1910. Über die dichteste Zusammenstellung von kongruenten Kreisen in einer Ebene. Dybwad in Komm., Oslo.

Wei, G., Mangal, S., Denman, J., Gengenbach, T., Lee Bonar, K., Khan, R.I., Qu, L., Li, T., Zhou, Q. (Tony), 2017. Effects of coating materials and processing conditions on flow enhancement of cohesive acetaminophen powders by high-shear processing with pharmaceutical lubricants. J. Pharm. Sci. 106, 3022–3032. https://doi.org/10.1016/J.XPHS.2017.05.020

Yang, J., Sliva, A., Banerjee, A., Dave, R.N., Pfeffer, R., 2005. Dry particle coating for improving the flowability of cohesive powders. Powder Technol. 158, 21–33. https://doi.org/10.1016/j.powtec.2005.04.032

Yang, Q., Ma, Y., Zhu, J., 2015. Applying a novel electrostatic dry powder coating technology to pellets. Eur. J. Pharm. Biopharm. 97, 118–124. https://doi.org/10.1016/J.EJPB.2015.10.006

Zhang, Q., Yang, J., Teng, S., Dave, R.N., Zhu, L., Wang, P., Young, M.W., Gogos, C.G., 2009. In-situ, simultaneous milling and coating of particulates with nanoparticles. Powder Technol. 196, 292–297. https://doi.org/10.1016/J.POWTEC.2009.08.011

Zhou, Q., Armstrong, B., Larson, I., Stewart, P.J., Morton, D.A.V., 2010. Improving powder flow properties of a cohesive lactose monohydrate powder by intensive mechanical dry coating. J. Pharm. Sci. 99, 969–981. https://doi.org/10.1002/jps.21885

Zhou, Q.T., Qu, L., Larson, I., Stewart, P.J., Morton, D.A.V., 2011. Effect of mechanical dry particle coating on the improvement of powder flowability for lactose monohydrate: a model cohesive pharmaceutical powder. Powder Technol. 207, 414–421. https://doi.org/10.1016/J.POWTEC.2010.11.028